Chapter 4

Porous Carbon Materials as Supreme Metal-Free Counter Electrode for Dye-Sensitized Solar Cells

Mohammad Aftabuzzaman and Hwan Kyu Kim

Additional information is available at the end of the chapter

http://dx.doi.org/10.5772/intechopen.75398

Abstract

Counter electrode (CE), as one of the key components of dye-sensitized solar cells (DSSCs), plays a significant role in the overall efficiency and cost of the device. Platinum metal has long been considered one of the most efficient CEs for DSSCs, but its scarcity, high cost, and low stability in I^-/I_3^- redox couple limit its application in the large scale. In this chapter, we provide a broad overview on porous carbon materials as supreme metal-free counter electrode for DSSCs. In the first part, we concisely discuss on the importance and working principle of DSSCs and then the influence of counter electrode on the photovoltaic performance of DSSCs. Afterward, we review different synthetic methods and precursors of porous carbon materials and their efficiency in DSSCs. In the last section, we discuss in detail with example how to characterize and evaluate the device performance using porous carbon materials as counter electrode. Finally, we finish this chapter with a brief summary and outlook of porous carbon materials as counter electrodes in DSSCs.

Keywords: porous carbon, synthesis, characterization, counter electrode, dye-sensitized solar cells

1. Introduction

As the third-generation solar cells, dye-sensitized solar cell (DSSC) is one of the most promising alternatives to the silicon solar cells, due to their simple assembly procedure, good plasticity, transparency, mechanical robustness, ability to work at wider angles, and in low light and environmental friendliness [1, 2]. After a significant breakthrough in the photoelectric conversion efficiency (7.1–7.9%) of DSSCs in 1991, through introducing mesoporous film of

TiO_2 nanocrystalline to adsorb dye instead of planar semiconductor electrode by O'Regan and Grätzel research group [3], DSSCs have stimulated a great research interest over the following 25 years and attained an efficiency of ca. 14% [4, 5].

The working principle of DSSCs is not similar to conventional solar cell, but it is similar to natural photosynthesis process where light absorption and charge carrier transportation have different substances, as shown in **Figure 1**. DSSCs consist of three important components: dye-coated TiO_2 film, counter electrode (CE), and electrolyte (or redox shuttle). In the DSSCs, after photoexcitation of sensitized dye, electrons from the LUMO level of dye molecule are injected into the conduction band of semiconductor metal oxide. Then, electrons transport to the anode and flow to the counter electrode (CE) via an external circuit. Finally, mediator electrolyte through reduction and oxidation carries electrons from counter electrode to the HOMO level of dye molecules, and dye is regenerated. This cycle is repeated again and again, and the device generates electric power continuously.

In this overall process of electron transfer, counter electrode plays a significant role on the photovoltaic parameters of DSSCs. The theoretical maximum photovoltage or open-circuit voltage of the DSSCs is higher than the output voltage after loading. This voltage loss is due to the mass transfer overpotential and the kinetic overpotential or charge transfer over potential. The former is mainly attributed to the ionic conductivity of electrolytes and the transportation of mediator species from the CE to the photoanode, whereas the latter is from the electrocatalytic activity of the CE surface toward mediator [6, 7]. The catalytic activity of the CEs can be

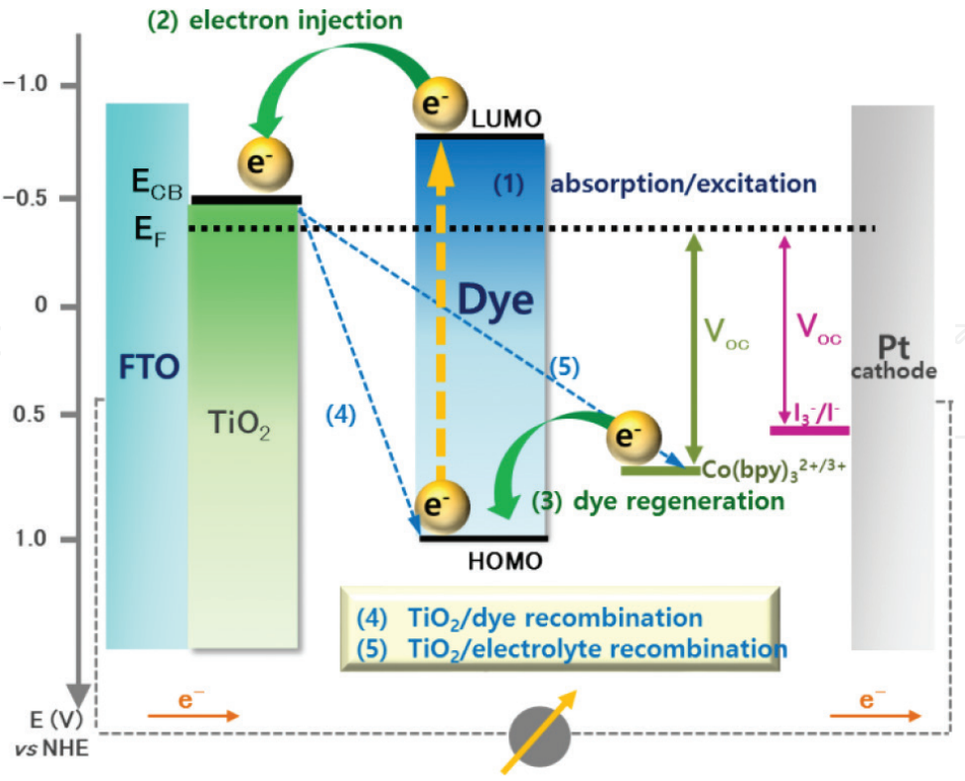

Figure 1. Schematic representation of the working principle of DSSCs.

explained in terms of current density J_o which is calculated from the charge transfer resistance (R_{ct}) by Eq. (1):

$$J_o = \frac{RT}{nFR_{ct}} \tag{1}$$

where R, T, n, and F are the gas constant, the temperature, the number of electrons transferred in the elementary electrode reaction ($n = 2$), and the Faradays constant, respectively.

The overall performance of solar cell is evaluated by the solar-to-electrical energy conversion efficiency, η, which is given by Eq. (2):

$$\eta = \frac{J_{SC} V_{OC} FF}{P_{in}} \tag{2}$$

where J_{sc} is the short-circuit current, V_{oc} is the open-circuit voltage, FF is the fill factor, and P_{in} is the incident light intensity. FF depends on the charge transfer resistance, on series resistance, as well as on the overvoltage for diffusion and electron transfer. Low charge transfer resistance, series resistance, and overvoltage for diffusion and electron transfer lead to a higher FF value, thus resulting in greater efficiency and pushing the output power of the solar cell closer toward its theoretical maximum.

As low-cost and environmentally friendly materials, porous carbon has high surface area, high catalytic activity, high stability in I^-/I_3^- redox shuttle, and better performance than the Pt CEs. The goal of this chapter is to discuss about the synthesis, characterization, and photovoltaic performance of porous carbon materials as supreme counter electrode for DSSCs.

2. Porous carbon materials as counter electrodes for DSSCs

As counter electrode (CE) is one of the most crucial components regulating the efficiency of DSSCs by catalyzing the reduction of the redox couples used as mediators to regenerate the sensitizer after electron injection, it is important to find a low-cost, high-efficiency, easy scalability, and corrosion-stable counter electrode. Platinum (Pt) has been widely employed as the standard CE in DSSCs due to its high catalytic reduction for redox shuttles, good chemical stability, and high conductivity. However, Pt is an expensive and scarce noble metal, which causes a problem for its large-scale production.

Carbon materials are one of the promising substitutes of Pt CE due to their low cost, environmentally friendly, scale availability, high surface area, high catalytic activity, high electrical conductivity, high thermal stability, good corrosion resistance toward iodine, high reactivity for triiodide reduction, etc. In 1996, Kay and Grätzel first explored graphite-carbon black mixture as CE and achieved a power conversion efficiency of 6.7% [8]. Thereafter, intensive research efforts have been focused on carbonaceous materials, such as carbon black, mesoporous carbon, graphite [9], graphene [10, 11], carbon nanotubes [12–15], and carbon nanofibers [16–18], and they have been successfully employed as counter electrodes.

Among the carbonaceous materials, porous carbon materials have captured extensive attention as CE materials for DSSCs, owing to its exceptional properties, including ultrahigh surface areas, large pore volumes, and tunable pore sizes and shapes, and also exhibit nanoscale effects in their mesopore channels and on their pore walls. High surface areas provide a large number of reaction or interaction sites for surface- or interface-related processes such as adsorption and catalysis. Moreover, mesopore channels facilitate the transport of atoms, ions, and large molecules through the bulk of the material and assist to overcome charge transfer resistance [19, 20].

2.1. Synthetic methods of porous carbon materials and photovoltaic performance in DSSCs

Porous carbon materials are mainly produced by activation [21, 22] and templating [19, 23–25] methods from different precursors, and the efficiency of porous carbon electrodes depends on synthesis methods and precursors. The synthetic process of porous carbons by activation is simple, low-cost, and environmentally friendly. Also, activated carbons (ACs) have excellent chemical and thermal stability as well as relatively good electrical conductivity. ACs are derived from different types of carbon-rich organic precursors (coffee waste, wood, pitch, coal, polymers, etc.) by carbonization in inert atmosphere with subsequent physical and/or chemical activation or plasma surface treatment. Depending on the activation process and the used carbon precursors, a variety of ACs with different physicochemical properties and well-developed specific surface area (SSA) from 500 to 3000 $m^2\ g^{-1}$ have been prepared and used as CEs for DSSCs. The high surface area of activated carbons can considerably contribute to improving the catalytic activity of the CEs in DSSCs.

Imoto et al. firstly reported that porous carbon materials prepared with an activation process were superior to a Pt-sputtered electrode as the DSSC CEs. Moreover, they observed that the photovoltaic performance was strongly influenced by the roughness factor and the apparent charge transfer resistance of DSSC CEs. Generally, the roughness factor of the carbon electrode becomes larger when a porous carbon material with larger surface area was used. Thus, the photovoltaic performance was improved with increasing the roughness factor of the carbon-based CE. Also, the apparent charge transfer resistance for redox reaction of I^-/I_3^- couple on the porous carbon CE decreased with increasing the roughness factor. Therefore, back transfer of the photoinjected electrons to the oxidized dyes and/or I_3^- ions was inhibited which in turns improved the FF value significantly. Furthermore, the V_{oc} value for the carbon counter electrode compared to the Pt counter electrode was increased by about 60 mV, maybe because of a positive shift of the formal potential for I^-/I_3^- couple [26].

Nitrogen-doped porous carbon nanorods (N-PCNRs) with high accessible surface area were prepared by Wang group through carbonization of polyaniline (PANI) nanorods and consequent chemical activation and explored as the DSSC CEs. The unique combination of the porosity with high accessible surface area, nitrogen doping, and nanorod structure endows the N-PCNR electrode with an excellent electrocatalytic activity for the I_3^- reduction, which is illuminated by electrochemical measurement. Under simulated AM 1.5 illumination (100 mW cm^{-2}), the DSSC based on N-PCNR counter electrode achieves a conversion efficiency of 7.01%, which is nearly close to that of the cell based on Pt CE (7.25%).

http://dx.doi.org/10.5772/intechopen.75398

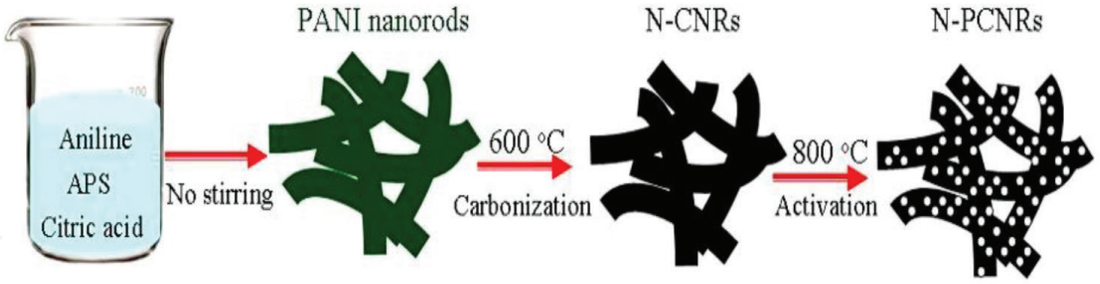

Figure 2. Preparation of nitrogen-doped porous carbon nanorods (N-PCNRs) [27] (copyright (2017) Elsevier).

In their experiment, PANI nanorods were firstly prepared by polymerization of aniline in aqueous solution using ammonium persulfate (APS) as the initiator, as shown in **Figure 2**. Ten grams of aniline and 7 g of citric acid were mixed in 500 mL of distilled water, and then 20 g of ammonium persulfate was dissolved in 150 mL of distilled water. Afterward, ammonium persulfate solution was added into the mixture solution of aniline and citric acid with vigorous stirring. The resulting solution was left standing at about 3°C for 20 h. The obtained dark green sample was filtered and washed with distilled water and then dried under vacuum at 50°C. The as-prepared PANI nanorods were pyrolyzed at 600°C under nitrogen atmosphere for 3 h to obtain nitrogen-doped carbon nanorods (N-CNRs). Finally, N-PCNRs were prepared by activating N-CNRs with KOH [27].

Recently, H. K. Kim group synthesized anchovy-derived nitrogen and sulfur Co-doped porous carbons (AnCs) by a simple carbonization and alkali activation method for DSSC CEs, as shown in **Figure 3**. Typically, a three-step strategy was used to prepare the activated carbon. Firstly, a dried anchovy powder was weighed and transferred into a quartz tubular furnace and then pre-carbonized at 300°C for 1 h under atmosphere, yielding a pre-carbonized material. An activation and carbonization process was sequentially carried out as follows: The pre-carbonized material was mixed with various mass ratios of KOH and then directly heated at an elevated temperature (700, 800, 900°C) for 2 h under inert nitrogen atmosphere. Finally,

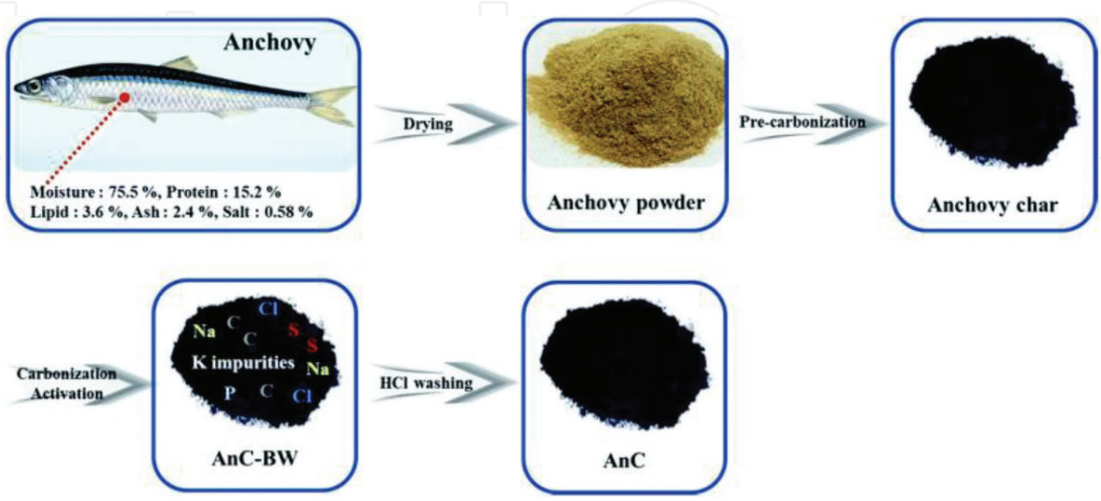

Figure 3. Approximate composition of a dried anchovy powder and schematic illustration for the preparation of anchovy-derived nitrogen and sulfur co-doped porous carbon materials [28] (copyright (2017) Royal Society of Chemistry).

the anchovy-derived activated carbon obtained was washed several times with aqueous 2 M HCl solution and deionized water in order to remove the potassium compounds and any impurities. After filtration, the samples were dried at 70°C in an electric vacuum oven.

The anchovy-derived activated carbons as a DSSC CE exhibited superior PCE of 12.72% to the Pt CE with 12.23%. It is ascribed to an improved fill factor caused by its better electrocatalytic ability [28]. To the best of our knowledge, this PCE is the highest efficiency value reported for DSSCs based on carbon nanomaterial-based CEs. **Table 1** summarizes porous carbon materials produced by activation and their precursors with photovoltaic performance.

Although activated carbon possesses high surface area, but most of the pores are micropore which may increase diffusion impedance of electrolytes into the pore of CEs especially for the bulkier redox couples like $Co(bpy)_3^{2+/3+}$. Templating method is used to synthesize mesopore and macropore carbon materials with connected channel. Depending on the template used, templating method can be classified into two classes: hard template and soft template. Typically, silica nanoparticles, zeolites, anodic aluminum oxide (AAO) films, and mesoporous silica have been used as the hard templates. The synthetic process involves the impregnation of carbon precursor into the porous structure of pre-synthesis template following the carbonization and removal of the template. On the other hand, soft templating involves the self-assembly of copolymers and their direct removal through carbonization. Various commercially available triblock copolymers PEO-PPO-PEO (PO, propylene oxide; EO, ethylene oxide), such as F127 ($EO_{106}PO_{70}EO_{106}$), P123 ($EO_{20}PO_{70}EO_{20}$), and F108 ($EO_{132}PO_{50}EO_{132}$), have been extensively used as the soft templates.

Hierarchical nanostructured carbon with a hollow macroporous core of ca. 60 nm in diameter in combination with mesoporous shell of ca. 30 nm in thickness was synthesized and explored as CE in metal-free organic dye-sensitized solar cells exhibited in **Figure 4** [33]. The superior

CE	Precursor	Dye-electrolyte	R_{ct} (Ω cm^2)	FF (%)	J_{sc} (mA cm^{-2})	PCE (%)	PCE-Pt (%)	Reference
AnCs	Anchovy	SM-315-$Co(bpy)_3^{2+/3+}$	7.56	75.9	18.78	12.72	12.23	[28]
Carbon chunks	Coffee waste	N719-I^-/I_3^-	0.46	72.6	15.09	8.32	8.07	[21]
N-PCNRs	Polyaniline	N719-I^-/I_3^-	2.2	63.0	15.85	7.01	7.25	[27]
HPC	Pine cone	N719-I^-/I_3^-		51.6	13.51	4.98	6.25	[29]
a-NCs	Resol	N719-I^-/I_3^-	7.5	55.0	17.92	6.9	7.1	[30]
Porous carbon	Commercial	N719-I^-/I_3^-	2.2	67.5	15.5	6.1	7.0	[31]
Flexible carbon	Commercial	N719-I^-/I_3^-	0.9	67.3	13.3	6.17	6.37	[32]
Bellfine AP	Commercial	N719-I^-/I_3^-		60.7	7:93	3.89	3.61	[26]

Table 1. Carbon materials produced by activation and their precursors with photovoltaic performance.

http://dx.doi.org/10.5772/intechopen.75398

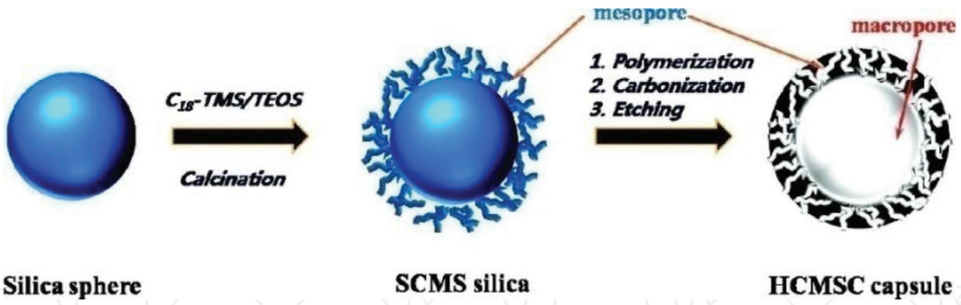

Figure 4. Typical synthetic scheme for HCMSC capsule [33] (copyright (2010) American Chemical Society).

structural characteristics, particularly, the unique hierarchical core/shell nanostructure along with 3D large interconnected interstitial volume with large specific surface area and mesoporous volume, were observed compared with other porous carbon counterparts such as activated carbons and ordered mesoporous carbon CMK-3 (fabricated by replication through nano-casting of SBA-15 silica and using phenol as the carbon source) and Pt counter electrode. This hierarchical core/shell nanostructural feature with 3D large interconnected interstitial volume facilitates mass transportation in hollow macroporous core/mesoporous shell carbon (HCMSC), which was synthesized by replicating through nano-casting of solid core/mesoporous shell silica and phenol and paraformaldehyde as precursor, and enables HCMSC to have highly boosted catalytic activity toward the reduction of I_3^- and so substantially enhanced photovoltaic performance. HCMSC as a DSSC CE displays a V_{oc} of 0.74 V, which is superior to that of the Pt CE by 20 mV. Moreover, it also exhibits a fill factor of 0.67 and an energy conversion efficiency of 7.56%, which are markedly higher than those of its carbon counterparts and comparable to that of Pt (i.e., fill factor of 0.70 and conversion efficiency of 7.79%). In addition, superb chemical stability was observed by HCMSC in the liquid electrolyte containing I^-/I_3^- redox couples, and its initial efficiency of ca. 87% was attained by the HCMSC counter electrode-based solar cell, even after 60 days of aging.

Gokhale et al. introduced a laser photochemical process to synthesize broccoli-type hierarchical morphology for use as a metal-free CE in DSSCs. The method includes pulsed excimer laser irradiation on a thin layer of liquid halo-aromatic organic solvent containing o-dichlorobenzene (DCB). The obtained coating reflects a self-assembled carbon nanoparticle and process-controlled morphology that yields a PCE of 5.1% which was comparable to the PCE of 6.2% with the conventional Pt-based counter electrode [24].

Wang et al. designed and fabricated a novel bioinspired Pt- and FTO-free integrated pure carbon counter electrode for DSSCs with orderly mesoporous carbon (OMC) as the catalytic layer and a porous carbon sheet as a conducting substrate (see in **Figure 5**). On a porous conducting substrate, a stiff, crustose lichen-like, integrated carbon-carbon architectured composite as a catalytic layer was made by a sequential process of spin coating, infiltration, and pyrolysis of polymer precursor. To fabricate the integrated pure carbon electrode, porous carbon plates (PCPs) were firstly prepared by a bulk molding-carbonization process using cheap coal powder as precursor. The permeation of electrolyte through the porous substrate has been fairly resolved by impermeable pretreatment through a repeat pitch impregnation-carbonization treatment of paraffin-protected PCPs. A phenol-formaldehyde resin solution including

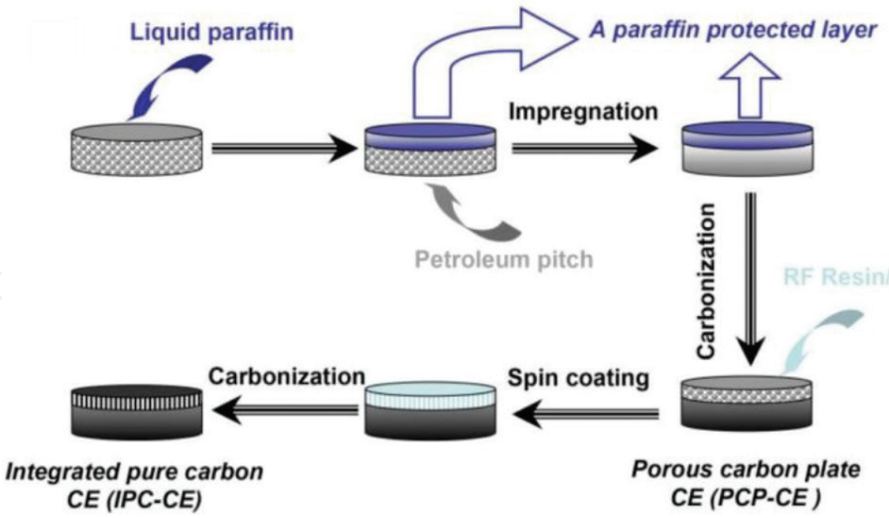

Figure 5. The fabrication procedure of the integrated pure carbon counter electrode for DSSCs [34] (copyright (2013) Royal Society of Chemistry).

Pluronic F127 ($EO_{106}PO_{70}EO_{106}$) as a template was spin coated onto the open pore side of the conductive substrate and then carbonized at 800°C under inert nitrogen atmosphere. By an evaporation-induced self-assembly (EISA) mechanism, an identical mesostructured resin film was formed. Successively, a catalytic mesoporous carbon layer that was embedded in the porous carbon plate was produced by carbonization. The architecturally integrated carbon-based CE displays very low charge transfer resistance (R_{ct}), owing to the large specific surface area of the OMC layer that is accessible to the redox couple, and low series resistance (R_s), due to the high conductivity of the carbon sheet (sheet resistance of 488 mΩ cm^{-1}). The values of R_s and R_{ct} are far lower than those of the platinized fluorine-doped tin oxide glass (Pt/FTO) electrode. DSSCs with this CE show higher PCE of 8.11% than the Pt/FTO-based devices with the PCE of 8.16% [34].

Heteroatom-doped mesoporous carbons have received a great attention because of their enhanced electrocatalytic activity resulted from heteroatoms [35, 36]. The electrocatalytic properties of these systems are typically attributed to high charge polarization arising from the difference in electronegativity between carbon and heteroatom leading to enhanced charge transfer capability and thus increased catalytic activity. Also, to enhance the ordered graphitic layer and stability, porous carbon materials are mixed with polymer, transition metal, and other nanocarbon materials like graphene and CNTs [37–41].

Wang et al. synthesized activated N-doped porous carbons (a-NCs) by pyrolysis and alkali activation of graphene-incorporated melamine formaldehyde resin (MF). To prepare a-NCs, firstly a homogeneous mixture of activated graphene (a-G) with melamine and formaldehyde was prepared and pre-carbonized in Teflon-lined autoclave at 140°C for 4 h to form graphene-incorporated MF resin. The as-prepared graphene-incorporated MF resin composite then carbonized at 800°C for 2 h in N_2 atmosphere followed by activation with KOH, yielding a-NCs. a-NCs with the moderate N-doping level, mesopore-rich porous texture, and incorporation of graphene enable the applications of a-NCs in electrode materials with high specific surface area and good conductivity for dye-sensitized solar cell (DSSCs). At the

http://dx.doi.org/10.5772/intechopen.75398

optimum activation temperature of 700°C, the obtained sample, labeled as a-NC700, possesses a satisfactory graphitization, a specific surface area of 1302 m^2 g^{-1} and an N fraction of 4.5%. A PCE of 6.9% is reached, when as-prepared a-NC700 used as a DSSC CE, which is comparable to that of the Pt CE-based DSSC (7.1%) [30].

H. K. Kim group prepared copolymer-templated nitrogen-enriched nanocarbons (CTNCs) and observed the better PCEs for both I^-/I_3^- and $Co(bpy)_3^{2+/3+}$ redox couples. CTNCs were synthesized by the pyrolysis of PAN-b-PBA copolymer as shown in **Figure 6**.

The block copolymer was pyrolyzed at 600–1000°C for 0.5 h under N_2 gas flow (150 mL min^{-1}) at a heating rate of 10°C min^{-1}, after stabilization through the cross-linking of the PAN block at 280°C for 1 h under air flow (150 mL min^{-1}) at a heating rate of 1°C min^{-1}, purged with N_2 gas for 1 h during cooling. Superior performance in catalytic activity toward the reduction of $Co(bpy)_3^{2+/3+}$ compared to the conventional Pt CE was observed. The detected remarkable activity of CTNCs is owing to their distinctive electronic properties stemming from the presence of nitrogen heteroatoms placed on the edges of nanographitic domains in combination with high specific surface area delivered by a three-dimensional, hierarchical pore structure. Overall, the application of CTNC CEs enhanced the efficiency and fill factor (FF) of JK-306 dye and $Co(bpy)_3^{2+/3+}$ redox couple-based DSSCs at one sun illumination, up to 10.32 and 73.5%, respectively, suggesting the substantial potential of these materials as an striking substitute to expensive Pt-based CEs [42].

Hasin group prepared Co or Ni species incorporated N-doped mesoporous carbon (Co-N-MC or Ni-N-MC) with high specific surface area and observed brilliant electrocatalytic activity toward the electrochemical reaction of I^-/I_3^- redox couple in DSSC systems as compared with N-doped mesoporous carbon (N-MC) displayed in **Figure 7**.

Co-N-MC and Ni-N-MC were synthesized on the basis of replication through nano-casting of SBA-15 mesoporous silica. The polymerization of aniline was conducted in the pore of SBA-15 mesoporous silica functionalized with alkyldiamine group. Cobalt(II) or nickel(II) ion was doped in the polyaniline (PANI) within the pores of SBA-15 followed by pyrolyzing in

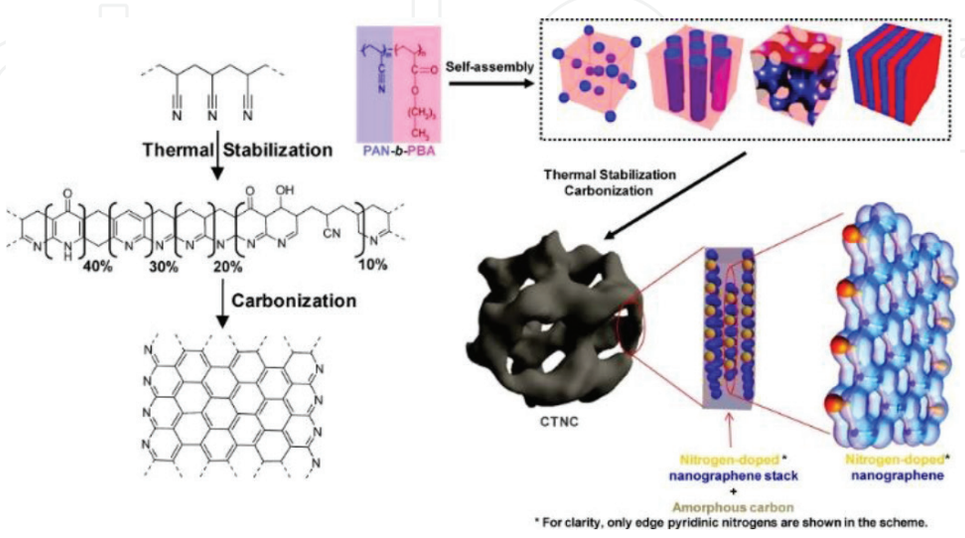

Figure 6. Schematic representation of preparation of CTNC [42] (copyright (2015) Royal Society of Chemistry).

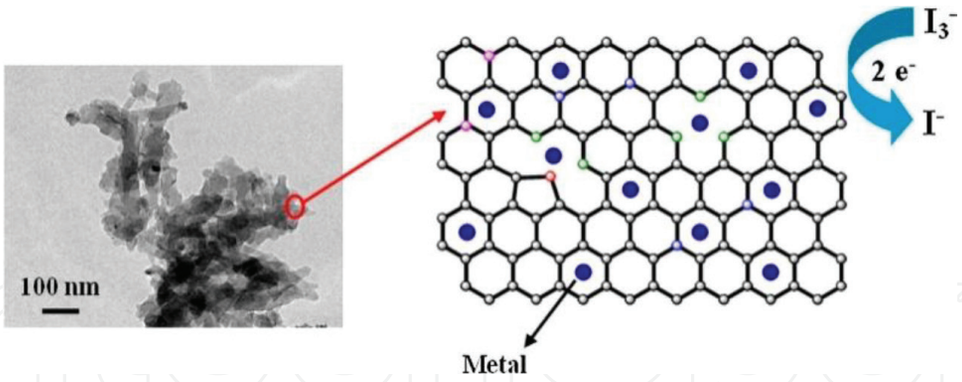

Figure 7. Immobilized Co or Ni on N-doped mesoporous carbons [43] (copyright (2017) Elsevier).

quartz tube. The considerable photoelectric conversion efficiency of Co-N-MC- and Ni-N-MC-based DSSCs is ascribed to the good electrical conductivity in their frameworks and the dominating contents of pyridinic and quaternary N species over pyrrolic N in their structural configuration. Furthermore, significantly lower charge transfer resistance (R_{ct}) associated with metal doping of the Co-N-MC and Ni-N- MC and excellent structural surface properties can also be responsible to enhance the photovoltaic performance. The fill factor (FF) and power conversion efficiency (η) of DSSC utilizing Ni-N-MC counter electrode (FF = 0.70 and η = 8.42%) were higher compared to the DSSC using platinized counter electrode (FF = 0.66 and η = 8.22%). Additionally, Ni-N-MC counter electrode exhibited good electrochemical stability after experiencing ten CV cycles. Moreover, compared to platinized electrode in catalyzing the T_2/T^- organic redox system, all N-MC, Co-N-MC, and Ni-N-MC show better performance. The integration of electrocatalytic Co or Ni species and N-doped mesoporous carbon matrix is an alternative approach for counter electrode electrocatalyst to diminish the cost of DSSCs [43]. Precursors and photovoltaic performance of porous carbon materials synthesized by soft- and hard-templating methods are summaries in **Tables 2** and **3**, respectively.

2.2. Morphological and structural characterization of porous carbon materials

The morphology of porous carbon materials is usually characterized by using scanning electron microscopy (SEM) or field emission scanning electron microscopy (FE-SEM) and transmission electron microscopy (TEM). **Figure 8**(**a**)–(**c**) shows the FE-SEM images for the surface morphology and microstructures of honeycomb-like activated porous carbons (HPCs) [29]. As shown in **Figure 8**(**a**), the micro-sized particles of the as-prepared sample revealed a honeycomb-like morphology containing a huge number of minute holes over its entire frameworks. Magnified view of FE-SEM image of the sample confirmed the interconnected macroporous structures with sizes of ~100–600 nm (in **Figure 8**(**b**)). Moreover, a close inspection reveals that the pore and surface wall of HPC sample comprised of many mesopores and micropores as shown in **Figure 8**(**c**). In addition, the TEM image in **Figure 8**(**d**) also confirmed the honeycomb-like morphology with the porous property.

X-ray diffraction (XRD) and Raman spectroscopy are used to ascertain the extent of crystallinity in the structure of porous carbon samples. Porous carbon materials display diffraction peaks at about 24 and 44°, which are the equivalent of hexagonal graphitic 002 (2θ = 24°) and

CE	Precursor	Dye-electrolyte	R_{ct} (Ω cm²)	FF (%)	J_{sc} (mA cm^{-2})	PCE (%)	PCE-Pt (%)	Reference
CTNC	PBA-b-PAN	JK-306-$Co(bpy)_3^{2+/3+}$	0.31	73.5	14.57	10.32	9.80	[42]
		JK-306-I^-/I_3^-		72.9	14.58	7.88		
HPCs	Resol	N719-I^-/I_3^-	4.68	65.0	14.97	7.22	7.25	[25]
MC	Resol	N719-I^-/I_3^-	17.2	61.0	14.32	6.06	6.29	[19]
OMC	Coal powder	N719-I^-/I_3^-	6.99	73.0	14.26	8.11	8.16	[34]
Broccoli-carbon	O-dichlorobenzene	N719-I^-/I_3^-		46.1	13.86	5.1	6.2	[24]
HPC	Resol	N719-I^-/I_3^-	0.3	67.0	15.44	6.48	6.45	[44]
OMC	Resol	Thiocyanate-I^-/I_3^-	6.5	68.0	14.13	7.69	8.25	[45]
MC	Resol	N3-I^-/I_3^-	0.7	65.0	15.5	6.18	6.26	[46]

Table 2. Porous carbon material synthesis by soft template and their precursors with photovoltaic performance.

101 (2θ = 44°) crystal planes as shown in **Figure 9**(**a**) [50]. To identify the degree of graphitization, Raman spectra are used as follows: Two peaks at 1340 and 1590 cm^{-1} that is assigned to the D band and G band are observed as shown in **Figure 9**(**b**).

The breathing mode vibration of A_{1g}, associated with the disordered carbon or defective graphitic carbon appeared at around 1353 cm^{-1} corresponding to the D band. Another peak related to the G band appeared at around 1590 cm^{-1}, which specifies the in-plane stretching vibration mode of E_{2g} in sp^2 sp^2C–C bond vibrations, as in graphitic phase [51].

CE	Precursor	Dye-electrolyte	R_{ct} (Ω cm²)	FF (%)	J_{sc} (mA cm^{-2})	PCE (%)	PCE-Pt (%)	Reference
Carbon framework	Quinoline	N719-I^-/I_3^-	0.14	69.0	16.54	8.75	7.55	[36]
S-PC	Pitch	N719-I^-/I_3^-	3.99	67.0	14.98	6.97	7.28	[47]
NMC	Resol	N719-I^-/I_3^-		60.0	15.46	7.02	7.26	[35]
MSU-F–C	Resol	N719-I^-/I_3^-	8.75	70.0	14.95	8.18	8.85	[48]
HCMSC	Resol	N719-I^-/I_3^-	0.5	67.0	16.86	7.56	7.79	[49]
Fe-MCF-C	Divinylbenzene	N719-I^-/I_3^-		69.0	14.70	7.89		[23]

Table 3. Porous carbon material synthesis by hard template and their precursors with photovoltaic performance.

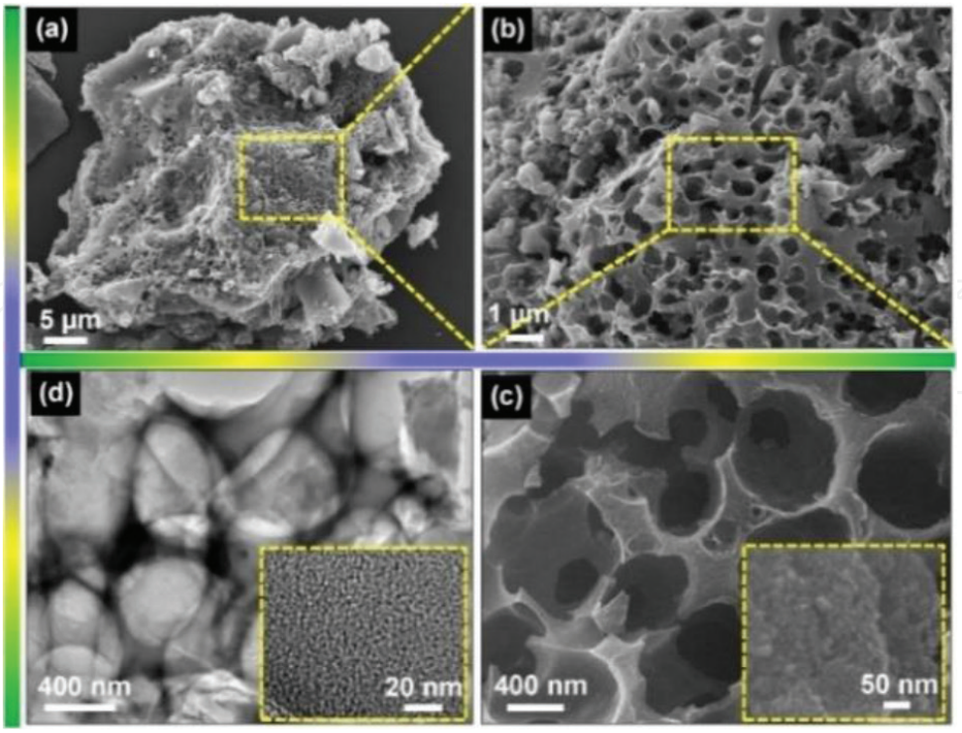

Figure 8. (a–c) FE-SEM images and (d) TEM images of the carbonized HPC sample under inert gas atmosphere [29] (copyright (2017) Elsevier).

Additionally, X-ray photoelectron spectroscopy (XPS) analysis gives the information about the presence of surface functional groups in the porous carbon. In **Figure 9**(**c**), the high-resolution XPS spectrum of C1s in the binding energy range between 280 and 288 eV revealed several carbon-based functional groups, which are assigned to the C–OH, C–C/C–H, C–O, and C=O bonds, respectively. Meanwhile, as shown in **Figure 9**(**d**), the deconvoluted XPS spectra of the O 1 s exhibited the three distinct peaks at the binding energies of 526–538 eV, which are attributed to the C–OH, C=O groups and chemisorbed water molecules, respectively [29].

The surface area and pore volume of porous carbon materials are measured through the experiments of adsorption-desorption isotherms, as shown inset in **Figures 9**(**a**) and **10**(**b**). Porous carbon materials typically exhibit III/IV isotherms with pronounced hysteresis loops, indicating the larger surface area.

The specific surface area is calculated from the Brunauer-Emmett-Teller (BET) equation, and the pore size distribution is derived from the desorption branches of the isotherms using the Barrett-Joyner-Halenda (BJH) method (**Figure 10**(**b**)) [52].

2.3. Electrochemical characterization of porous carbon material-based counter electrodes

The catalytic properties of counter electrodes in DSSCs are usually characterized by electrochemical impedance spectroscopy (EIS) [53, 54]. EIS measurements are performed in a symmetric thin-layer cell (called dummy cell) comprising two identical electrodes and same electrolyte used in the full DSSCs. The Nyquist plots for porous carbon CE consist of three

http://dx.doi.org/10.5772/intechopen.75398

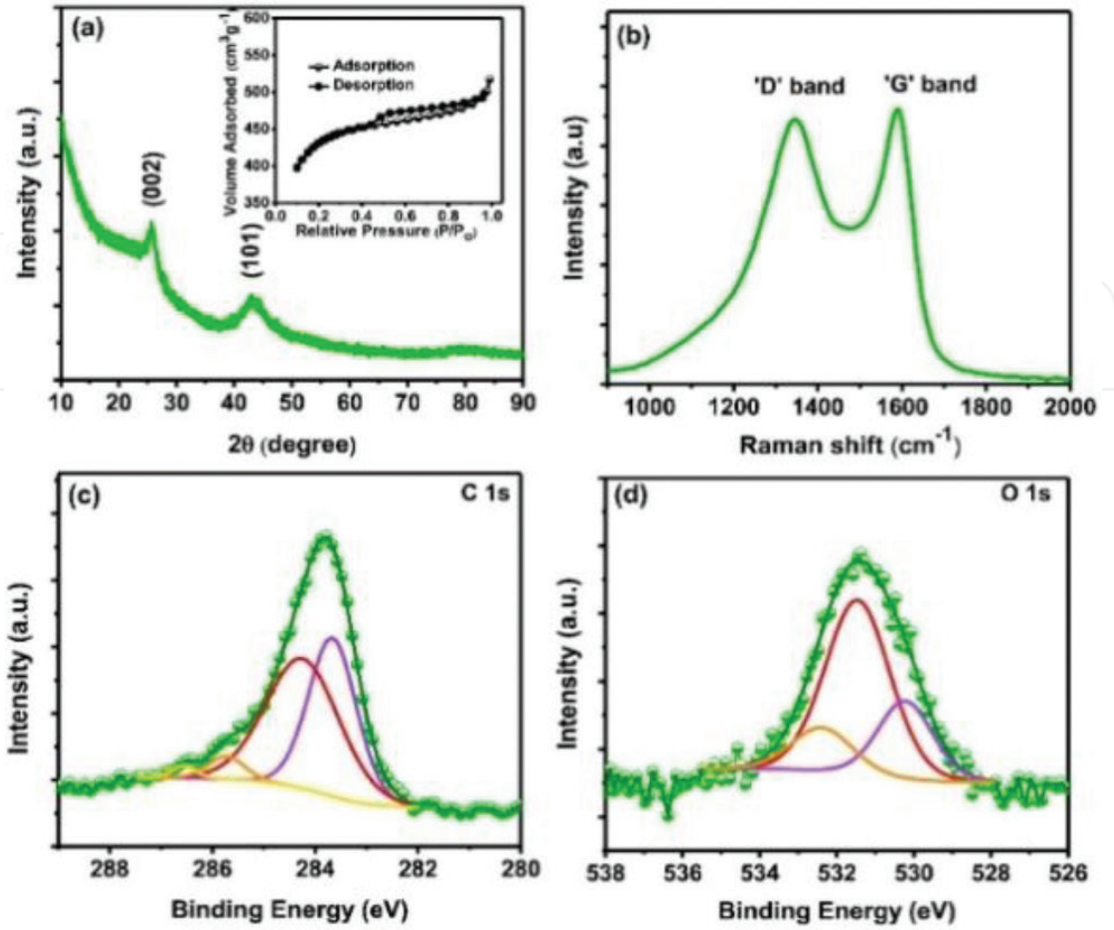

Figure 9. (a) XRD pattern, (b) Raman spectrum, and (c-d) XPS spectra of the HPC sample. The inset of (a) shows the nitrogen adsorption–desorption isotherm of the HPC sample [29] (copyright (2017) Elsevier).

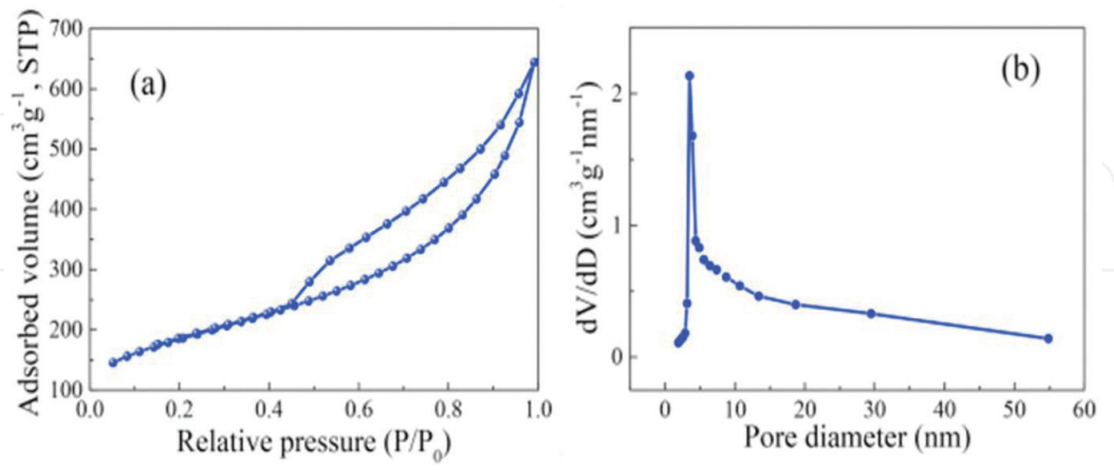

Figure 10. Nitrogen adsorption-desorption isotherms (a) and BJH pore-sized distributions (b) of the S-PC [47] (copyright (2015) Elsevier).

semicircles, which are assigned in the order of increasing frequency to the Nernst diffusion impedance in the bulk electrolyte (< 10 Hz), the charge transfer processes at the electrode/electrolyte interface (2500–25 Hz), and the Nernst diffusion impedance in the pores of electrode materials (100–2.5 KHz) in **Figure 11**(**a**).

The equivalent circuit elements for fitting the EIS data, which is well known as a Randles-type equivalent circuit, comprise of the ohmic serial resistance (R_s), the resistance-capacitance (RC) network consisting of the charge transfer resistance (R_{ct}) and the corresponding capacitance (C) at the electrode/electrolyte interface, and the Nernst diffusion impedance in the bulk electrolyte (N_{bulk}) between electrodes and the pores of electrode materials (N_{pore}) as shown in **Figure 11**(**b**) [55]. The impedance spectrum of the Pt/electrolyte interface diverges to some extent from the behavior of a RC network with an ideal capacitance owing to the roughness of the TCO substrate surface. This effect can be defined by a term called as "constant phase element (CPE)." The impedance Z_{CPE} of a CPE is given by Eq. (3) [53, 56]:

$$Z_{CPE} = B(i\omega)^{-\beta} \tag{3}$$

where ω is the angular frequency, B is the CPE parameter, and β is the CPE exponent ($0 \leq \beta \leq 1$, for ideal capacitance $\beta = 1$).

The parameter N_{pore} can be omitted for Pt CE where the catalytic reaction occurs on virtually nonporous surface (the equivalent circuit for the symmetric cell comprising of Pt CEs is shown in the inset of **Figure 11**(**a**)). As a result, the Nyquist plot for Pt electrode exhibits two semicircles, allocating in the order of decreasing frequency to the charge transfer process at Pt electrode/electrolyte interface and Nernst diffusion of redox couple in electrolyte. From the

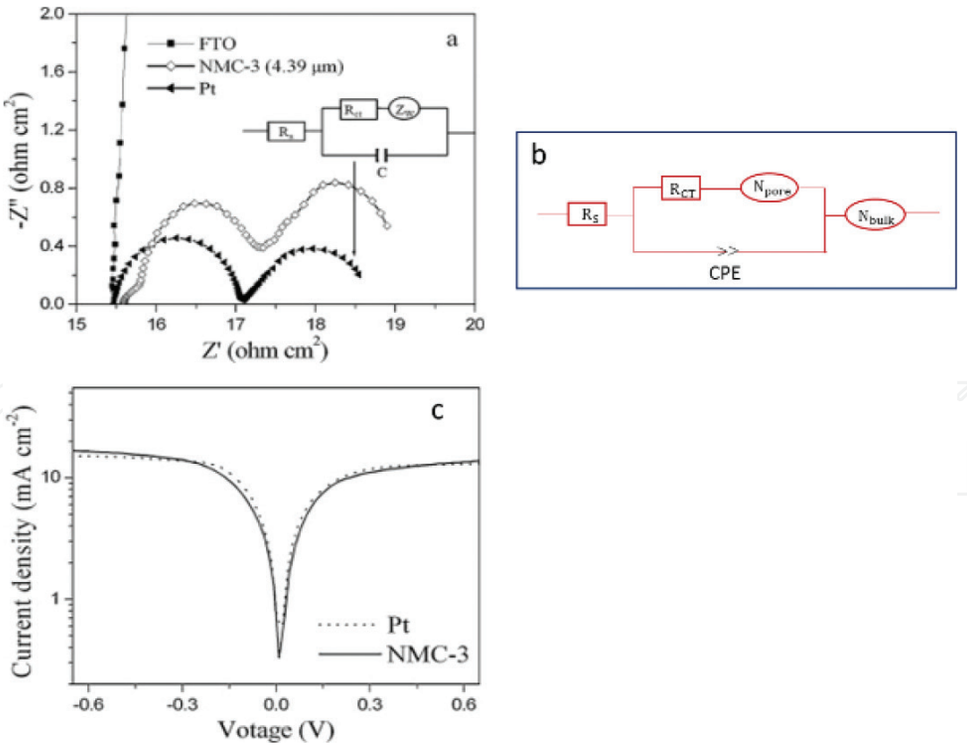

Figure 11. (a) Nyquist plots of the symmetric cells consisting of FTO glass, NMC-3, and Pt electrodes, respectively, equivalent circuit element for Pt CE in the inset. (b) Equivalent circuit element for NMC-3 porous carbon. (c) Tafel polarization curves of the symmetric cells fabricated with two identical Pt and NMC-3 electrodes [35] (copyright (2013) Elsevier).

diameter of the high-frequency semicircle, R_{ct} value of the Pt CE can be estimated directly. The charge transfer resistance, R_{ct}, of the porous carbon CEs depends on the thickness of electrodes. The data listed in **Table 4** show that the R_{ct} of NMC-3 electrode decreases with increasing thickness of NMC-3 layer. R_{ct} value of NMC-3 electrode decreases by 10.36 Ω cm^2 (from 11.81 to 1.45 Ω cm^2), once the thickness of NMC-3 layer increases by 3.44 m (from 0.95 to 4.39 m). This result is mainly owing to the increase in active surface area of NMC-3 film with the thicker NMC-3 layer.

Nevertheless, R_{ct} value barely changes with additional increase of the thickness of NMC-3 layer. The optimum thickness of NMC-3 layer is 4.39 m, which is considerably lower than that of the commonly studied carbon nanoparticle CE in DSSCs. Also, R_s value does not change significantly with the thickness of NMC-3 layer. This is due to the preparation of NMC-3 electrodes on the same FTO substrate, and also the R_s value is controlled mainly by the electrical properties of the FTO substrate. Capacitance, *C*, increases systematically with the thickness of NMC-3 layer as expected due to an increase in active surface area.

Lower R_{ct} denotes more efficient reduction of redox couples at the CE-electrolyte interface, which in turn reduces charge recombination process and increases the dye-regeneration process at the dye-coated TiO_2/electrolyte interface. Electrochemically active surface areas (EASAs) were estimated from the results of chronoamperometric (CA) measurements according to the Randles-Sevcik equation to expose the question of whether the lower R_{ct} originates from an intrinsically higher catalytic activity or the high surface area of porous carbon [42]. It was found that the intrinsically higher catalytic activity of porous carbon electrodes was mainly responsible for lower charge transfer at the interface.

Tafel polarization measurements are carried out in a symmetric cell similar to the one used in EIS experiment. Usually, the Tafel curve comprises of three distinguishable zones, the polarization zone at low potential (voltage range of −120 to 120 mV), the Tafel zone at middle potential (with a sharp decrease), and the diffusion zone at high potential (horizontal part). The exchange current density (J_o), which is directly associated to the electrocatalytic ability of an electrode, can be calculated by extrapolating the intercept of the anodic and cathodic branches of the corresponding curves in the Tafel zone. **Figure 11**(**c**) displays the Tafel polar-

Thickness of NMC layer (μm)	R_s (Ω)	R_{ct} (Ω cm^2)	C (μF cm^{-2})
0.95	15.41	11.81	15.8
1.68	15.44	7.75	26.9
3.16	15.45	4.09	34.6
4.39	15.52	1.45	42.6
6.53	15.57	1.5	49.7

Table 4. Electrochemical impedance parameters for NMC-3 electrode with various thicknesses of carbon layer (35) (copyright (2013) Elsevier).

ization curves of the NMC-3 and electrodepositing Pt electrodes. The cathodic and anodic branches of the Tafel curves show a steep slope for NMC-3 and Pt electrodes, indicating a high J_o on the surface of NMC-3 and Pt electrodes. This implies that NMC-3 can have an electrocatalytic ability as effective as Pt electrode toward the I^-/I_3^- redox reaction. Furthermore, the limiting diffusion current density of the NMC-3 and Pt electrodes is observed to be of the same magnitude. This result describes that the bimodal mesopore structure can deliver an advantageous network for the diffusion of the electrolyte.

Furthermore, cyclic voltammetry of dummy cell is used to verify the electrocatalytic activity of porous carbon. The peak-to-peak separation (E_{pp}) and the peak current are two important parameters for comparing catalytic activities of both CEs. A smaller E_{pp} and larger peak currents indicate higher catalytic performance. **Figure 12(a)–(b)** shows the comparison of the CV curves of CTNC-800 and Pt electrodes in the $Co(bpy)_3^{2+/3+}$ system acquired at different scan rates (25–200 mV s^{-1}).

EIS is also used to check the stability of porous carbon CEs. **Figure 13(a)** and **(b)** shows the electrochemical stability of the dummy cells with CTNC-800 and Pt CEs under cumulative potential cycling with $Co(bpy)_3^{2+/3+}$ in acetonitrile. After 100 cycles, although only a very modest increase of R_{ct} values was observed from 0.35 to 0.45 Ω cm^2 for CTNC-800 CEs, but for Pt CEs, the R_{ct} values increased from 3.10 to 11.26 Ω cm^2 by nearly 400%. The sluggish decline of R_{ct} for CTNC-800 compared to Pt clearly implies the higher stability of CTNC-800 in the acetonitrile $Co(bpy)_3^{2+/3+}$ electrolyte as shown in **Figure 13(c)**. Superior electrochemical stability of

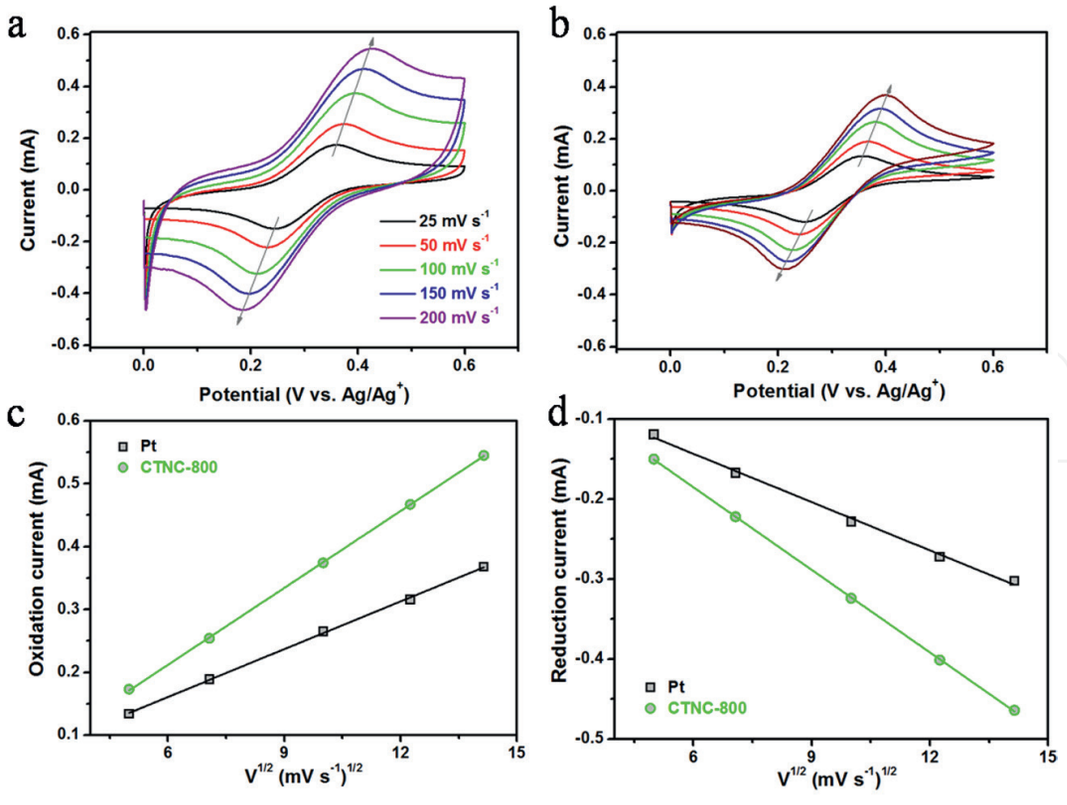

Figure 12. Cyclic voltammograms using CTNC-800 (a) and Pt (b) cathodes in with various scanning rates. The oxidation (c) and reduction (d) peak currents with respect to the square root of scanning rate [42]. Copyright (2015) Royal Society of Chemistry.

CTNC-800 was also confirmed by the EIS measurements of dummy cells after aging the two electrodes at room temperature and open circuit in **Figure 13(d)**. The EIS curve of the CTNC-800 electrode over the period of 14 days was nearly unchanged, while the EIS curves for Pt showed evidence of a progressive increase of the resistance upon aging.

The greater slopes of the linear dependence of the reduction and oxidation currents against the square root of potential and higher peak current of CTNC-800 electrodes at all scan rate confirm the better catalytic activity of CTNC-800 toward the reduction of $Co(bpy)_3^{2+/3+}$ than the Pt CE.

2.4. Photovoltaic performance evaluation of DSSCs with porous carbon CEs

To evaluate the photovoltaic performance of DSSCs employing porous carbon CEs, generally a prescribed amount of carbon materials is grounded in a mortar with 0.1 ml tetrabutyl titanate and 8 ml n-butanol to obtain the carbon paste. Then, the electrode is prepared by coating carbon paste on FTO glass using doctor-blade method and heated at a certain temperature for 30 min. On the other hand, photoanode is prepared by depositing TiO_2 film with the thickness of 10 μm on FTO glass substrate by doctor-blade method and then sintered at a certain tem-

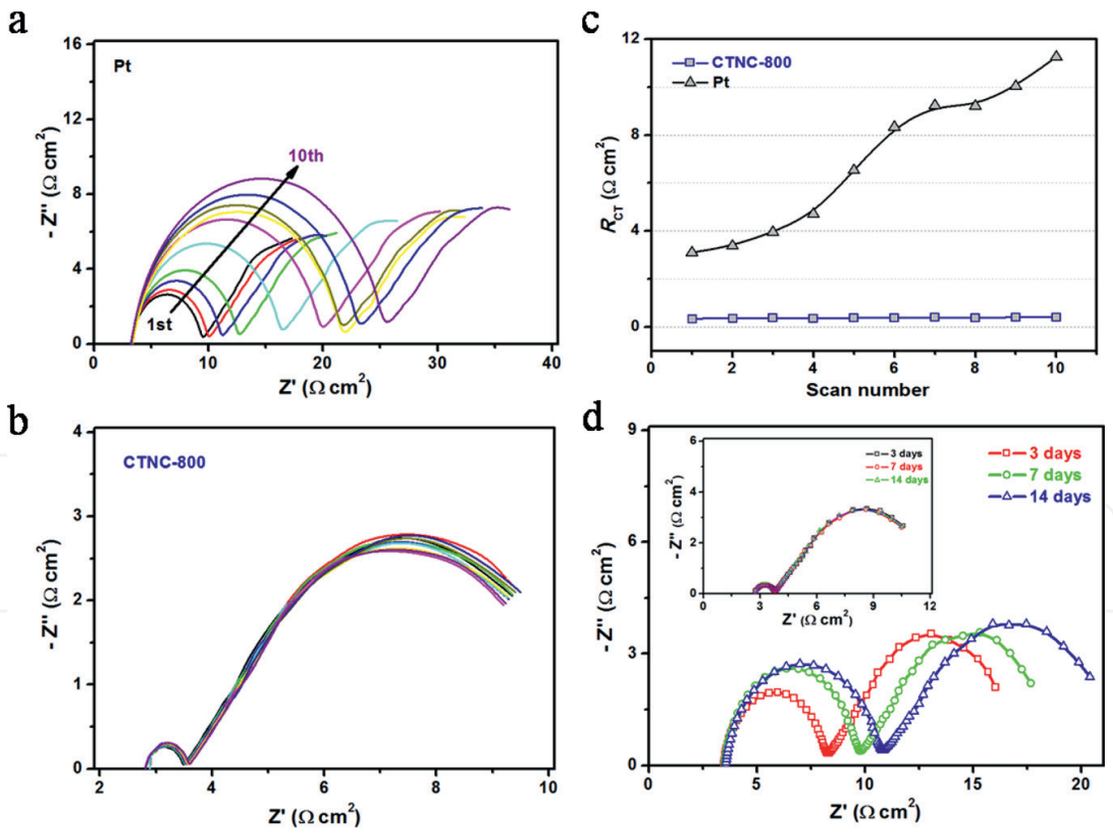

Figure 13. Electrochemical stability under potential-cycling on dummy cells with Pt (a), CTNC-800 (b) in acetonitrile solution of . The sequence of measurements was as follows: 10 × CV scans (from 0V → 1V → 1V → 0V → 1 V, scan rate 50) followed by 30 s relaxation at 0 V followed by an EIS measurement at 0 V from Hz to0.1 Hz. This sequence of electrochemical stability testing was repeated 10 times. (c) changes in the Pt and CTNC-800 according to the potential cycling. (d) Nyquist plots of symmetrical dummy cells consisting of Pt and CTNC-800 (inset) collected after 3 days (black), 7 days (red) and 14 days (green) of aging at room temperate and open circuit [42]. Copyright (2015) Royal Society of Chemistry.

perature for 30 min. After that, the sintered TiO_2 electrodes are immersed into a solution containing dye in ethanol for a long time at room temperature to adsorb dye on TiO_2 photoanode.

A DSSC device is fabricated by clamping a dye-sensitized TiO_2 photoanode, a drop of electrolyte, and a counter electrode. For I^-/I_3^- redox shuttle, a mixture of 0.5 M 1-methyl-3-propylimidazolium iodide, 0.3 MLiI, 0.06 M I_2, and 0.4 M 4-tert-butylpyridine in 3-methoxypropionitrile is used as the electrolyte of DSSCs [35]. Finally, the photovoltaic performance of DSSC device is evaluated under AM 1.5 solar simulator illumination at 100 mW cm^{-2}.

Figure 14 compares the photocurrent density-voltage (*J-V*) curves of the DSSCs with NMC-3, Pt, and FTO glass counter electrodes. The photovoltaic parameters of the DSSCs, including short-circuit current density (J_{sc}),), open-circuit voltage (V_{oc}), fill factor (FF), and power conversion efficiency (η), are summarized in **Table 5**. The DSSC with FTO glass as counter electrode exhibits a V_{oc} of 0.49 V, a J_{sc} of 4.13 mA cm^{-2}, and a FF of 0.10, leading to a poor power conversion efficiency of 0.20%. When NMC-3 porous carbon material is employed as the counter electrode in DSSC, the DSSC attains a V_{oc} of 0.71 V, J_{sc} of 15.46 mA cm^{-2}, FF of 0.64, and η of 7.02%. This power conversion efficiency is considerably comparable to 7.26% of the DSSC with Pt counter electrode. The outstanding photovoltaic performances of the DSSCs with NMC-3 counter electrode mostly originate from the vivid electrocatalytic performance of NMC-3 electrode associated with the nitrogen doping, bimodal mesopore structure, and large surface area.

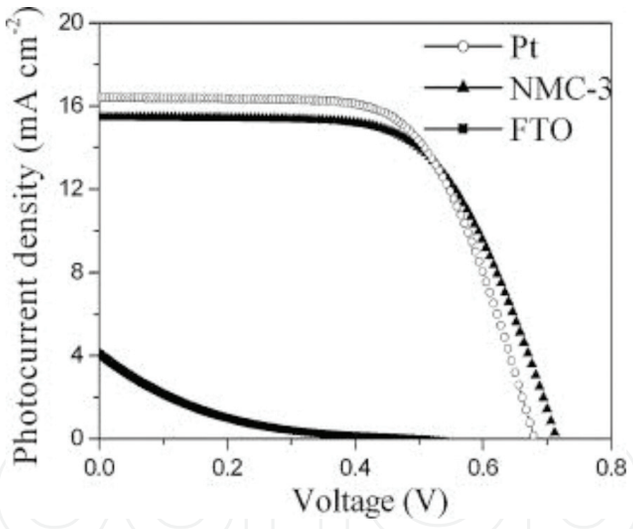

Figure 14. Photocurrent density-voltage curves of DSSCs with Pt, NMC-3, and FTO glass counter electrodes [35] (copyright (2013) Elsevier).

Counter electrode	V_{oc} (V)	J_{sc} (mA cm^{-2})	FF	η (%)
Pt	0.68	16.43	0.65	7.26
NMC-3	0.71	15.46	0.64	7.02
FTO	0.49	4.13	0.10	0.20

Table 5. Photovoltaic parameters of the DSSCs using Pt, NMC-3, and FTO glass counter electrode [35] (copyright (2013) Elsevier).

3. Conclusions and outlook

Dye-sensitized solar cells (DSSCs) have aroused intense interest and been regarded as one of the most prospective solar cells, due to low-cost, flexibility, simple device fabrication, and high conversion efficiency under weak light, in comparison to the conventional photovoltaic devices. Very recently, G2E in Swiss and G24i in the UK including Korean and Japan companies have demonstrated commercial and prototyped components based on DSSC technology with liquid electrolytes. However, the unit costs, long-term device stability, and power conversion efficiency must be further improved for real-life applications. For this purpose, considerable efforts have been devoted to the search for low-cost Pt-free catalysts that exhibit high electrochemical activity and fast electron transfer kinetics, while a platinum (Pt) metal is still known as the highly efficient and extensively used counter electrode (CE) in DSSCs; however, it has more or less problems that make it improper for the real-life application in DSSCs, such as its high manufacturing cost owing to its natural scarcity and insufficient long-term instability to the I^-/I_3^- redox couple in DSSCs. As a result, significant efforts have been devoted to finding possible alternatives to Pt, including carbon blacks, carbon nanotubes, functionalized graphene, and heteroatom-doped graphene nanoplatelets as efficient metal-free electrocatalysts. An ideal counter electrode in DSSCs must possess the following properties: high electrocatalytic ability and high conductivity, optimum thickness, high surface area and porous nature, low charge transfer resistance, high electrochemical and mechanical stability, energy level that matches the potential of the redox couple electrolyte, high reflectivity, and good adhesivity with TCO. High electrocatalytic ability and low charge transfer resistance of CEs increase FF and J_{sc} and subsequently PCE of the DSSC. In this chapter, porous carbon materials have been considered as one of the promising candidates for the alternative to PT CE, since they have high surface area and porous nature, chemical corrosion resistance, electrochemical and mechanical stability, low cost, and simple preparation methods compared to Pt counter electrodes. Especially, heteroatom-doped porous carbon materials, such as CTNCs and AnCs, exhibited better electrocatalytic ability, lower charge transfer resistance, and higher PCE than the Pt CEs in $Co(bpy)_3^{2+/3+}$-based electrolyte which make them promising candidates as metal-free CE for DSSCs and open a new research area for porous carbon CEs in $Co(bpy)_3^{2+/3+}$-based DSSCs. However, they are not sufficiently active in iodide electrolytes, which are more common and desirable electrolytes. In the future, better electrocatalytic ability and electrochemical stability of carbon-based materials toward both redox couples of iodide and cobalt electrolytes still need to be significantly improved for the practical application of DSSCs.

Acknowledgements

This work was supported by the National Research Foundation of Korea (NRF) grant funded by the Korean government (MSIT) through the Mid-career Researcher Program (2017R1A2A1A17069374), the Functional Districts of the Science Belt Support Program (2017K000494), and the Korea Research Institute of Chemical Technology (KRICT & Project No. KK1702-A00).

Author details

Mohammad Aftabuzzaman and Hwan Kyu Kim*

*Address all correspondence to: hkk777@korea.ac.kr

Global GET-Future Lab and KU-KRICT CRC, Department of Advanced Materials Chemistry, Korea University, Sejong, Korea

References

[1] Zhang Q, Park K, Xi J, Myers D, Cao G. Recent progress in dye-sensitized solar cells using nanocrystallite aggregates. Advanced Energy Materials. [Internet]. 2011 Nov 1 [cited 2017 Oct 6];**1**(6):988-1001. Available from: http://doi.wiley.com/10.1002/aenm.201100352

[2] Hagfeldt A, Boschloo G, Sun L, Kloo L, Pettersson H. Dye-sensitized solar cells [Internet]. Chemical Reviews. 2010 Nov 10 [cited 2017 Oct 8];**110**(11):6595-6663. Available from: http://pubs.acs.org/doi/abs/10.1021/cr900356p

[3] O'Regan B, Grätzel M. A low-cost, high-efficiency solar cell based on dye-sensitized colloidal TiO2 films. Nature [Internet]. 1991 Oct 24 [cited 2017 Oct 6];**353**(6346):737-740. Available from: http://www.nature.com/doifinder/10.1038/353737a0

[4] Eom YK, Kang SH, Choi IT, Yoo Y, Kim J, Kim HK. Significant light absorption enhancement by a single heterocyclic unit change in the π-bridge moiety from thieno[3,2-b] benzothiophene to thieno[3,2-b]indole for high performance dye-sensitized and tandem solar cells. Journal of Materials Chemistry A [Internet]. 2017;**5**(5):2297-2308. Available from: http://xlink.rsc.org/?DOI=C6TA09836C

[5] Kakiage K, Aoyama Y, Yano T, Oya K, Fujisawa J, Hanaya M. Highly-efficient dye-sensitized solar cells with collaborative sensitization by silyl-anchor and carboxy-anchor dyes. Chemical Communication [Internet]. 2015;**51**(88):15894-15897. Available from: http://xlink.rsc.org/?DOI=C5CC06759F

[6] Li K, Yu Z, Luo Y, Li D, Meng Q. Recent progress of counter electrodes in nanocrystalline dye-sensitized solar cells. Journal of Materials Science & Technology [Internet]. 2007;**23**(5):577. Available from: http://d.wanfangdata.com.cn/periodical_clkxjsxbe200705001.aspx

[7] Papageorgiou N. Counter-electrode function in nanocrystalline photoelectrochemical cell configurations. Coordination Chemistry Reviews [Internet]. 2004 [cited 2017 Nov 1];**248**:1421-1446. Available from: https://ac.els-cdn.com/S0010854504000645/1-s2.0-S0010854504000645-main.pdf?_tid=8ab64572-becd-11e7-8ea1-00000aacb35f&acdnat=1509517748_8164d715bb1caf309a882f60b5800677

[8] Grätzel M, Kay A. Low cost photovoltaic modules based on dye sensitized nanocrystalline titanium dioxide and carbon powder. Sol Energy Mater Sol Cells [Internet]. 1996;**44**(1):99-117. Available from: http://linkinghub.elsevier.com/retrieve/pii/0927024896000633

[9] Wei YS, Jin QQ, Ren TZ. Expanded graphite/pencil-lead as counter electrode for dye-sensitized solar cells. Solid State Electron [Internet]. 2011;**63**(1):76-82. Available from: http://dx.doi.org/10.1016/j.sse.2011.05.019

[10] Kavan L, Yum JH, Grätzel M. Graphene nanoplatelets outperforming platinum as the electrocatalyst in co-bipyridine-mediated dye-sensitized solar cells. Nano Letters. 2011; **11**(12):5501-5506

[11] Kavan L, Yum JH, Nazeeruddin MK, Grätzel M. Graphene nanoplatelet cathode for Co(III)/(II) mediated dye-sensitized solar cells. ACS Nano. 2011;**5**(11):9171-9178

[12] Imbrogno A, Pandiyan R, Barberio M, Macario A, Bonanno A, El khakani MA. Pulsed-laser-ablation based nanodecoration of multi-wall-carbon nanotubes by Co-Ni nanoparticles for dye-sensitized solar cell counter electrode applications. Materials for Renewable and Sustainable Energy [Internet]. 2017;**6**(2):11. Available from: http://link.springer.com/10.1007/s40243-017-0095-3

[13] Siuzdak K, Klein M, Sawczak M, Wróblewski G, Słoma M, Jakubowska M, et al. Spray-deposited carbon-nanotube counter-electrodes for dye-sensitized solar cells. Physica Status Solidi (A) Applications and Materials. 2016;**213**(5):1157-1164

[14] Sedghi A, Nourmohammadi Miankushki H. Effect of Multi Walled carbon nanotubes as counter electrode on dye sensitized solar cells. International Journal of Electrochemical Science [Internet]. 2014;**9**:2029-2037. Available from: www.electrochemsci.org

[15] De Volder, Michael FL. Tawfick SH, Ray HB, A. John H. Carbon nanotubes: Present and future commercial applications. Science (80-). 2013;**339**(6119):535-539

[16] Yousef A, Brooks RM, El-Newehy MH, Al-Deyab SS, Kim HY. Electrospun Co-TiC nanoparticles embedded on carbon nanofibers: Active and chemically stable counter electrode for methanol fuel cells and dye-sensitized solar cells. International Journal of Hydrogen Energy [Internet]. 2017;**42**(15):10407-10415. Available from: http://dx.doi.org/10.1016/j.ijhydene.2017.01.171

[17] Guo H, Zhu Y, Li W, Zheng H, Wu K, Ding K, et al. Synthesis of highly effective Pt/carbon fiber composite counter electrode catalyst for dye-sensitized solar cells. Electrochim Acta [Internet]. 2015;**176**:997-1000. Available from: http://dx.doi.org/10.1016/j.electacta.2015.07.103

[18] Wang G, Kuang S, Zhang W. Helical carbon nanofiber as a low-cost counter electrode for dye-sensitized solar cells. Materials Letters [Internet]. 2016;**174**:14-6. Available from: http://dx.doi.org/10.1016/j.matlet.2016.03.076

[19] Chen M, Shao L-L, Qian X, Liu L, Ren T-Z, Yuan Z-Y. Mesoporous carbon counter electrode materials for dye-sensitized solar cells: The effect of structural mesopore ordering. Chemical Engineering Journal [Internet]. 2014;**256**:23-31. Available from: http://linkinghub.elsevier.com/retrieve/pii/S1385894714008523

[20] Jiang QW, Li GR, Wang F, Gao XP. Highly ordered mesoporous carbon arrays from natural wood materials as counter electrode for dye-sensitized solar cells. Electrochemistry Communications [Internet]. 2010;**12**(7):924-927. Available from: http://dx.doi.org/10.1016/j.elecom.2010.04.022

[21] Chung DY, Son YJ, Yoo JM, Kang JS, Ahn CY, Park S, et al. Coffee waste-derived hierarchical porous carbon as a highly active and durable electrocatalyst for electrochemical energy applications. ACS Applied Materials & Interfaces. 2017;**9**(47):41303-41313

[22] Zhao B, Huang H, Jiang P, Zhao H, Huang X, Shen P, et al. Flexible counter electrodes based on mesoporous carbon aerogel for high-performance dye-sensitized solar cells. Journal of Physical Chemistry C. 2011;**115**(45):22615-22621

[23] Ramasamy E, Lee J. Ferrocene-derivatized ordered mesoporous carbon as high performance counter electrodes for dye-sensitized solar cells. Carbon N Y [Internet]. 2010;**48**(13):3715-3720. Available from: http://dx.doi.org/10.1016/j.carbon.2010.06.033

[24] Gokhale R, Agarkar S, Debgupta J, Shinde D, Lefez B, Banerjee A, et al. Laser synthesized super-hydrophobic conducting carbon with broccoli-type morphology as a counter-electrode for dye sensitized solar cells. Nanoscale [Internet]. 2012;**4**(21):6730. Available from: http://xlink.rsc.org/?DOI=c2nr32082g

[25] Shao LL, Chen M, Yuan ZY. Hierarchical porous carbons as a metal-free electrocatalyst of triiodide reduction for dye-sensitized solar cells. Journal of Power Sources [Internet]. 2014;**272**:1091-1099. Available from: http://dx.doi.org/10.1016/j.jpowsour.2014.09.028

[26] Imoto K, Takahashi K, Yamaguchi T, Komura T, Nakamura JI, Murata K. High-performance carbon counter electrode for dye-sensitized solar cells. Solar Energy Materials & Solar Cells. 2003;**79**(4):459-469

[27] Wang G, Yan C, Hou S, Zhang W. Low-cost counter electrodes based on nitrogen-doped porous carbon nanorods for dye-sensitized solar cells. Materials Science in Semiconductor Processing [Internet]. 2017;**63**(November 2016):190-195. Available from: http://dx.doi.org/10.1016/j.mssp.2017.02.018

[28] Kim CK, Choi IT, Kang SH, Kim HK. Anchovy-derived nitrogen and sulfur co-doped porous carbon materials for high-performance supercapacitors and dye-sensitized solar cells. RSC Advances [Internet]. 2017;**7**(57):35565-35574. Available from: http://dx.doi.org/10.1039/C7RA06102A%0Ahttp://xlink.rsc.org/?DOI=C7RA06102A

[29] Nagaraju G, Lim JH, Cha SM, Yu JS. Three-dimensional activated porous carbon with meso/macropore structures derived from fallen pine cone flowers: A low-cost counter electrode material in dye-sensitized solar cells. Journal of Alloys and Compounds [Internet]. 2017;**693**:1297-1304. Available from: http://dx.doi.org/10.1016/j.jallcom.2016.10.015

[30] Wang L, Gao Z, Chang J, Liu X, Wu D, Xu F, et al. Nitrogen-doped porous carbons as electrode materials for high-performance supercapacitor and dye-sensitized solar cell. ACS Applied Materials & Interfaces. 2015;**7**(36):20234-20244

[31] Li K, Luo Y, Yu Z, Deng M, Li D, Meng Q. Low temperature fabrication of efficient porous carbon counter electrode for dye-sensitized solar cells. Electrochemistry Communications [Internet]. 2009;**11**(7):1346-1349. Available from: http://dx.doi.org/10.1016/j.elecom.2009.04.025

[32] Chen J, Li K, Luo Y, Guo X, Li D, Deng M, et al. A flexible carbon counter electrode for dye-sensitized solar cells. Carbon N Y [Internet]. 2009;**47**(11):2704-2708. Available from: http://dx.doi.org/10.1016/j.carbon.2009.05.028

[33] Fang B, Fan SQ, Kim JH, Kim MS, Kim M, Chaudhari NK, et al. Incorporating hierarchical nanostructured carbon counter electrode into metal-free organic dye-sensitized solar cell. Langmuir. 2010;**26**(13):11238-11243

[34] Wang C, Meng F, Wu M, Lin X, Wang T, Qiu J, et al. A low-cost bio-inspired integrated carbon counter electrode for high conversion efficiency dye-sensitized solar cells. Physical Chemistry Chemical Physics [Internet]. 2013;**15**(34):14182. Available from: http://xlink.rsc.org/?DOI=c3cp52525b

[35] Wang G, Kuang S, Wang D, Zhuo S. Nitrogen-doped mesoporous carbon as low-cost counter electrode for high-efficiency dye-sensitized solar cells. Electrochim Acta [Internet]. 2013;**113**:346-353. Available from: http://dx.doi.org/10.1016/j.electacta.2013.09.107

[36] Xiao N, Song J, Wang Y, Liu C, Zhou Y, Liu Z, et al. Nitrogen-doped porous carbon with well-balanced charge conduction and electrocatalytic activity for dye-sensitized solar cells. Carbon N Y. 2018;**128**:201-204

[37] Li L, Sui H, Zhang W, Li X, Yang K, Hagfeldt A, et al. Mesoporous carbon-imbedded W_2C composites as flexible counter electrodes for dye-sensitized solar cells. Journal of Materials Chemistry C [Internet]. 2016;**4**:6778-6783. Available from: http://xlink.rsc.org/?DOI=C6TC01601D

[38] Selamat MH, Ahmad AH. Application of dye-sensitized solar cell (Dssc) from polyurethane (Pu)/diol-nai electrolyte with activated carbon (Ac) composite electrode. 2016;**10**(2):2-4

[39] Shao L-L, Chen M, Ren T-Z, Yuan Z-Y. Ordered mesoporous carbon/graphene nanosheets composites as counter electrodes in dye-sensitized solar cells. Journal of Power Sources [Internet]. 2015;**274**:791-798. Available from: http://linkinghub.elsevier.com/retrieve/pii/S0378775314017169

[40] Chen M, Shao L-L, Qian X, Ren T-Z, Yuan Z-Y. Direct synthesis of cobalt nanoparticle-imbedded mesoporous carbons for high-performance dye-sensitized solar cell counter electrodes. Journal of Materials Chemistry C [Internet]. 2014;**2**(48):10312-10321. Available from: http://xlink.rsc.org/?DOI=C4TC02270J

[41] Park S-H, Jung H-R, Kim B-K, Lee W-J. MWCNT/mesoporous carbon nanofibers composites prepared by electrospinning and silica template as counter electrodes for dye-sensitized solar cells. Journal of Photochemistry and Photobiology A: Chemistry [Internet]. 2012;**246**:45-49. Available from: http://linkinghub.elsevier.com/retrieve/pii/S101060301200384X

[42] Ju MJ, Choi IT, Zhong M, Lim K, Ko J, Mohin J, et al. Copolymer-templated nitrogen-enriched nanocarbons as a low charge-transfer resistance and highly stable alternative to platinum cathodes in dye-sensitized solar cells. Journal of Materials Chemistry A [Internet]. 2015;**3**(8):4413-4419. Available from: http://xlink.rsc.org/?DOI=C4TA07012G

[43] Hasin P, Amornkitbamrung V, Chanlek N. Economical nanocomposites of cobalt or nickel species and polyaniline-derived N-doped mesoporous carbons for dye-sensitized

solar cells as counter electrodes. Journal of Catalysis [Internet]. 2017;**351**:19-32. Available from: http://dx.doi.org/10.1016/j.jcat.2017.03.021

[44] Wang G, Huang C, Xing W, Zhuo S. Micro-meso hierarchical porous carbon as low-cost counter electrode for dye-sensitized solar cells. Electrochimica Acta [Internet]. 2011;**56**(16):5459-5463. Available from: http://dx.doi.org/10.1016/j.electacta.2011.03.024

[45] Ramasamy E, Chun J, Lee J. Soft-template synthesized ordered mesoporous carbon counter electrodes for dye-sensitized solar cells. Carbon N Y [Internet]. 2010;**48**(15):4563-4565. Available from: http://dx.doi.org/10.1016/j.carbon.2010.07.030

[46] Wang G, Xing W, Zhuo S. Application of mesoporous carbon to counter electrode for dye-sensitized solar cells. Journal of Power Sources. 2009;**194**(1):568-573

[47] Yang W, Ma X, Xu X, Li Y, Raj SI, Ning G, et al. Sulfur-doped porous carbon as metal-free counter electrode for high-efficiency dye-sensitized solar cells. Journal of Power Sources [Internet]. 2015;**282**:228-234. Available from: http://dx.doi.org/10.1016/j.jpowsour.2015.02.060

[48] Ramasamy E, Lee J. Large-pore sized mesoporous carbon electrocatalyst for efficient dye-sensitized solar cells. Chemical Communications [Internet]. 2010;**46**(12):2136. Available from: http://xlink.rsc.org/?DOI=b920916f

[49] Fan SQ, Fang B, Kim JH, Jeong B, Kim C, Yu JS, et al. Ordered multimodal porous carbon as highly efficient counter electrodes in dye-sensitized and quantum-dot solar cells. Langmuir. 2010;**26**(16):13644-13649

[50] Wickramaratne NP, Perera VS, Park BW, Gao M, McGimpsey GW, Huang SD, et al. Graphitic mesoporous carbons with embedded prussian blue-derived iron oxide nanoparticles synthesized by soft templating and low-temperature graphitization. Chemistry of Materials. 2013;**25**(14):2803-2811

[51] Sadezky A, Muckenhuber H, Grothe H, Niessner R, Pöschl U. Raman microspectroscopy of soot and related carbonaceous materials: Spectral analysis and structural information. Carbon N Y. 2005;**43**(8):1731-1742

[52] Cheng Q, Ji L, Wu K, Zhang W. Morphology-dependent electrochemical enhancements of porous carbon as sensitive determination platform for ascorbic acid, dopamine and uric acid. Scientific Reports [Internet]. 2016;**6**(January):1-8. Available from: http://dx.doi.org/10.1038/srep22309

[53] Hauch A, Georg A. Diffusion in the electrolyte and charge-transfer reaction at the platinum electrode in dye-sensitized solar cells. Electrochimica Acta. 2001;**46**(22):3457-3466

[54] Papageorgiou N. An iodine/triiodide reduction electrocatalyst for aqueous and organic media. Journal of the Electrochemical Society [Internet]. 1997;**144**(3):876. Available from: http://jes.ecsdl.org/cgi/doi/10.1149/1.1837502

[55] Roy-Mayhew JD, Bozym DJ, Punckt C, Aksay IA. Functionalized graphene as a catalytic solar cells. ACS Nano. 2010;**4**(10):6203-6211

[56] Córdoba-Torres P, Mesquita TJ, Nogueira RP. Relationship between the origin of constant-phase element behavior in electrochemical impedance spectroscopy and electrode surface structure. Journal of Physical Chemistry C. 2015;**119**(8):4136-4147